Intrusion-Extrusion Experiments of $MgCl_2$ Aqueous Solution in Pure Silica Ferrierite: Evidence of the Nature of Intruded Liquid by *in situ* High Pressure Synchrotron X-ray Powder Diffraction

Rossella Arletti[a], Laura Ronchi[b], Simona Quartieri[c], Giovanna Vezzalini[d], Andrey Ryzhikov[b], Habiba Nouali[b], T. Jean Daou[b], Joël Patarin[b]

[a] Dipartimento di Scienze della Terra, Università di Torino, Via Valperga Caluso 35, Torino, Italy
[b] Université de Strasbourg (UDS), Université de Haute Alsace (UHA), Equipe Matériaux à Porosité Contrôlée (MPC), Institut de Science des Matériaux de Mulhouse (IS2M), UMR CNRS 7361, 3 bis rue Alfred Werner, F-68093 Mulhouse, France.
[c] Dipartimento di Scienze Matematiche e Informatiche, Scienze Fisiche e Scienze della Terra, Università di Messina, Viale Ferdinando Stagno d'Alcontres 31, 98166 Messina S. Agata, Italy
[d] Dipartimento di Scienze Chimiche e Geologiche, Università di Modena e Reggio Emilia, Via G. Campi 103, 41100 Modena, Italy

Corresponding Authors
Joël Patarin
*E-mail: joël.patarin@uha.fr Phone: +33 389 33 68 80. Fax: +33 389 33 68 85.

Rossella Arletti
*E-mail: rossella.arletti@unito.it Phone: +39 01 16 70 51 29. Fax: +39 01 16 70 51 28.

ABSTRACT

Experimental intrusion-extrusion isotherms of $MgCl_2 \bullet 21H_2O$ solution were recorded at room temperature on pure silica FER-type zeolite (Si-FER). The intrusion occurs at 195 MPa and the phenomenon is completely reversible with a slight hysteresis. The "Si-FER - $MgCl_2$ aqueous solution" system behaves like a spring. The material was deeply characterized before and after intrusion-extrusion experiments and no significant changes were observed. The unit cell parameters were refined – on the basis of the in situ synchrotron X-ray powder diffraction data - up to 1.47 GPa and then at P_{amb} upon pressure release. The Rietveld refinement of the data collected at 0.28 GPa (280 MPa), a pressure close to the intrusion value, shows that both ions and water molecules present in the $MgCl_2$ aqueous solution were intruded in the porosities. However, the solvation degree of the intruded ions differs from the initial solution, revealing a partial desolvation of both magnesium and chloride ions. As a whole, the nature and amount of the intruded species correspond to a $MgCl_2 \bullet 10H_2O$ composition. Moreover, at a higher pressure (0.68 GPa), a phase transition from the orthorhombic P*mnn* to the monoclinic P$2_1/n$ s.g. is observed in Si-FER. At 1.47 GPa, the zeolite maintains this monoclinic symmetry, while another phase transition, to the monoclinic P2_1 s.g., is argued from the analysis of the pattern of the sample compressed to 2.6 GPa and then collected upon pressure release to ambient conditions.

KEYWORDS.

FER-type zeolite, pure silica ferrierite, intrusion-extrusion experiments, in-situ high pressure synchrotron XRPD experiments, structural refinement.

1. INTRODUCTION

The global demand for low cost, efficient and sustainable energy and environmental applications is ever increasing. This is largely driven by rapid discoveries and emerging innovations in the science and technology of materials. Since fifteen years, absorption or energy storage using pure-silica zeolites (zeosils) has been developed and opened a new field of applications for these exciting microporous solids [1-3]. The basic idea is in relation with the pressure induced hydration process (PIH) in microporous materials which is well documented [4-5] and focuses on the intrusion of water or aqueous salt solutions (non-wetting liquid) into a hydrophobic porous material. To penetrate the non-wetting liquid in such microporous matrices, a certain pressure must be applied [6]. During this forced penetration (intrusion), the mechanical energy can be converted into interfacial one. Depending on various physical parameters related to the porous material - such as its pore system (cavities or channels), its dimensionality (1, 2, or 3-D) or pore size - when the pressure is released (extrusion) the "zeosil-water" system is able to restore, dissipate or absorb the supplied mechanical energy accumulated during the compression step with a more or less significant hysteresis and, as a consequence, it displays a spring, shock-absorber or bumper behavior, respectively.

A large number of "zeosil-water" systems has already been studied [7-10]. More recently this research field was extended to metal-organic framework [11-14], but also to the intrusion of electrolytes [15-20]. With this type of liquid, the energetic performances of the "zeosil-liquid" systems were improved by a considerable increase of the intrusion pressure. Thus, the intrusion of 20M LiCl solution in pure silica MFI-type zeolite led to a rise of the intrusion pressure up to three times in comparison with pure water [16,17]. Several hypotheses were proposed to explain the increase of the intrusion pressure: (i) a higher solid-liquid interfacial tension [6], (ii) an ion desolvation phenomenon [21,22], (iii) a confinement effect of the

nanopore walls [23,24], or (iv) an osmotic phenomenon [25,26]. The intrusion of highly concentrated electrolyte solutions can also change the behavior of the "zeosil- aqueous solution" system. It was the case, for instance, for the LTA-and *BEA-type zeosil [27,19]. Thus, for the "*BEA zeosil-water" and "*BEA zeosil-10M LiCl aqueous solution" systems a bumper behavior is observed. In both cases, the intruded liquid is not expelled from the solid. From the elemental analysis of the corresponding solids, no lithium cations are detected. Therefore, the intruded liquid is pure water. Whereas, using concentrated LiCl aqueous solution (15-20 M) as non-wetting liquid, the system displays a shock-absorber behavior and, during the decompression step, the liquid is completely expelled from the porous solid [19]. It was supposed that this behavior change was related to a change of the nature of the intruded liquid from water, to solvated ions from highly concentrated LiCl aqueous solutions. Although numerous simulation works have been performed to understand the intrusion of concentrated electrolytes aqueous solutions in these solids [15], to our knowledge, at the present time, the nature of the intruded liquid is still questionable since no direct experimental observation has been made.

Understanding the changes in water structure and dynamics as a consequence of the interactions with confining hydrophobic surfaces is also relevant for the advances in fundamental sciences and in several technological applications. Examples are the uses for energy purposes and the selective adsorption processes of volatile organic compounds where pure-silica zeolites are used.

In the last decades a number of studies have been devoted to the structural investigation of zeolite-water systems, in particular in relation of the so-called "pressure induced hydration" [4,5,28,29]. Arletti et al. [29] studied the P-induced penetration of aqueous/alcohol (m.e.w.) mixture (16 methanol: 3 ethanol: 1 water) in the channel of an all-silica ferrierite (Si-FER) (FER Framework type [30]) by *in situ* high pressure (HP) X-ray powder diffraction (XRPD).

The structure of this zeolite displays a 2 dimensional channel system with 10- and 8 membered ring (MR) openings along the [001] and [010] directions, respectively. Thanks to the Rietveld refinements of *in situ* XRPD data, 15 water molecules were located in Si-FER channels at 200 MPa. On the contrary, no methanol or ethanol penetration was observed [29].

On the basis of these results, we decided to investigate the P-induced intrusion of electrolyte solutions with these aims: *i)* to answer the following question: would both ions and water molecules enter the porosity? Or, as observed for m.e.w. experiment, only water molecules are allowed to penetrate the channels? *ii)* to compare the elastic behavior of ferrierite when compressed with the selected electrolytic solution with that observed in the previous experiments performed with aqueous/alcohol solution.

In the present work, the energetic performances of Si- FER-type zeolite are studied by means of $MgCl_2 \bullet 21H_2O$ (2.65M) aqueous solution intrusion−extrusion experiments. $MgCl_2$ was selected as electrolyte - instead of the previously used LiCl - because of the higher diffusion factor of Mg cation, which makes the Rietveld refinement of the XRD data relative to the intruded system easier.

The samples, before and after such experiments, were fully characterized by conventional XRPD, thermogravimetric analyses and N_2 adsorption−desorption experiments. *In situ* HP synchrotron XRPD experiments were carried out to obtain structural information during the intrusion-extrusion process. To our knowledge, this is the first case of a detailed structural description of the nature and location of the species intruded under pressure in zeolite porosities using an electrolyte solution as penetrating medium.

2. EXPERIMENTAL SECTION

2.1 Synthesis of pure silica ferrierite

Si-FER sample was synthesized according to the procedure published by Kuperman et al. [31] in fluoride medium and using pyridine and propylamine as structure-directing agents. The reaction gel had the following molar composition: 1,5 SiO_2 : 2 HF-py : 4 propylamine : 16 pyridine : 8 H_2O. The reactants used were fumed silica (Aerosil 130), hydrogen fluoride–pyridine (HF-py, 70 wt.% HF in pyridine, Aldrich), pyridine (SDS, 99.5%), propylamine (Fluka, 99%) and distilled water. After homogenization (slight stirring), the mixture was introduced in a Teflon-lined stainless-steel autoclave and heated at 180 °C during 5 days. After synthesis, the product was filtered, washed with distilled water and dried at 60 °C overnight. The solid was then calcined at 880 °C to completely remove the organic template.

2.2 Intrusion−Extrusion Experiments

The intrusion−extrusion experiments with $MgCl_2 \bullet 21H_2O$ aqueous solution were performed at room temperature with the FER-type zeosil sample in the form of compressed and preliminary degassed pellets using a modified mercury porosimeter (Micromeritics Model Autopore IV), as described in our previous works [7]. The experimental intrusion−extrusion curves were obtained after subtraction of the curve corresponding to the compressibility of pure $MgCl_2$ aqueous solution. The values of the intrusion (P_{int}) and extrusion (P_{ext}) pressures correspond to that of the half volume total variation on the corresponding intrusion or extrusion isotherm. Pressure is expressed in megapascals (MPa) and volume variation in milliliters (mL) per gram of calcined samples. The experimental error on the pressure and on the volume is estimated to 1 %.

After intrusion−extrusion experiments, the samples were washed with water to remove traces of $MgCl_2$. The absence of chloride anions in the filtrate was checked by adding few drops of 1 M silver nitrate aqueous solution (no silver chloride precipitate was observed). Then the

samples were dried at 60 °C overnight, and hydrated in a 80 % relative humidity atmosphere for 24 h in order to set the hydration state.

2.3 X-ray Powder Diffraction experiments

2.3.1 XRPD experiments at ambient pressure.

X-ray diffraction patterns were collected, before and after intrusion, in a Debye−Scherrer geometry on a STOE STADI-P diffractometer equipped with a curved germanium (111), primary monochromator, and a linear position-sensitive detector (6 ° 2θ) using Cu $K\alpha_1$ radiation (λ = 0.15406 nm). Measurements were achieved for 2θ angle values in the 5−50 range, step 0.04 °, and time/step = 40 s.

2.3.2 In situ HP XRPD experiments.

In situ HP synchrotron XRPD experiments were performed on the SNBL1 (BM01a) beamline at ESRF (Grenoble), with fixed wavelengths of 0.7023 Å using modified Merril-Bassett DACs [32] and a $MgCl_2 \cdot 21H_2O$ aqueous solution as Pressure Transmitting Medium (PTM). Pressure was calibrated using the ruby fluorescence method [33] on the non-linear hydrostatic pressure scale [34]. The estimated precision in the P values is 0.05 GPa. The experiment was performed in the pressure range P_{amb} - 2.6 GPa. Some patterns were also collected upon decompression from the highest pressure to P_{amb}. The diffraction data were collected in the Debye–Scherrer geometry on Pilatus IP detectors (with pixel dimensions of 172 μm x 172 μm, respectively) at a fixed distance of 230 mm. One-dimensional diffraction patterns were obtained by integrating the two dimensional images with the program FIT2D [35].

Unit cell parameters were determined by Rietveld profile fitting up to 1.47 GPa. The data quality at higher pressure and the crystallization of a MgCl–bearing phase from the solution

prevented further refinements. The Si-FER sample underwent a phase transition from P*mnn* to P$12_1/n1$ *s.g.* above 0.28 GPa (280 MPa). The quality of the collected powder data allowed the structural refinement to converge successfully for the experiment at 0.28 GPa. On the pattern collected upon pressure release only a Lebail profile fitting was possible, due to the low quality of the data and the cell parameters were successfully refined in the P 12_11 *s.g.*

Rietveld profile fitting was performed using the GSAS package [36] with the EXPGUI [37] interface. The starting atomic coordinates were taken from the structural model [29] and the intruded extraframework species were located after the inspection of the Fourier Difference Map of the electronic density. The scattering curve to be used for each site was carefully chosen on the basis of the bond distances and of the mutually exclusions rules. For instance, being the distance among two equivalent atoms in position 0.5, 0.024, 0.125 (labelled Cl1 in table S2) 1.92 Å - too short to admit Mg-O, or Cl-O W-W bonds - the two equivalent positions could not be simultaneously occupied. Thus the occupancy factor of that site cannot exceed 50%. On the basis of the electronic density deriving from the map, the only admitted species is Cl. Mg was located in the site 0.5, 0.5, 0 on the basis of its distance and its coordination sphere with the other maxima found in the difference Fourier map. This position for Mg is also strongly consistent with the data resulting by the studies of natural zeolite ferrierite: in all the samples of this mineral phase this position is occupied by Mg in coordination with water.

The background curve was fitted by a Chebyshew polynomial with 20 coefficients. The pseudo-Voigt profile function proposed by Thomson et al. [38] was applied, and the peak intensity cut-off was set to 0.1 % of the peak maximum. Soft-restraints were applied to the T-O distances [Si-O = 1.58(2)-1.62(2) Å] and the weight was gradually decreased after the initial stages of refinement. The isotropic displacement parameters were constrained to the same value for all the tetrahedral cations and to a different value for all the framework oxygen

atoms. Being the refinement of partially occupied extraframework sites really challenging, several refinements were performed with different constraints on the thermal parameters to test possible correlations with the occupancy factors. A first one was performed constraining to the same value only U_{ISO} of water oxygen atoms and then refining: U_{ISO} resulted 0.33 for water molecules, 0.25 for Cl and 0.18 for Mg. and the fit was satisfactory. In a second refinement, the U_{ISO} of water molecules, Mg and Cl ions were fixed to 0.1: the occupancy factors only slightly changed (Cl occupancy passed from 0.52 to 0.48, Mg occupancy from 0.35 to 0.37, W1 occupancy from 1.1 to 0.94, that of W2 remained 1.0 and that of W3 passed from 0.24 to 0.20). The R factors of the fit, in these conditions, worsen, hence in the paper the refinement deriving from the first test is reported. The unit-cell parameters were allowed to vary for all the refinement cycles.

Observed and calculated profiles are reported in Figure 1, details of the structural refinements are reported in Table S1. The refined cell parameters as a function of pressure are reported in Table 1. Atomic coordinates, site occupancies and isotropic displacement parameters are reported in Table S2, and selected interatomic distances in Table S3.

2.4 Nitrogen Adsorption−Desorption Measurements

Nitrogen adsorption−desorption isotherms were performed at -196 °C using a Micromeritics ASAP 2420 apparatus. Prior to the adsorption measurements, the intruded−extruded samples, and the non-intruded sample, were outgassed at 90 °C overnight under vacuum to eliminate physisorbed water and to avoid the dehydroxylation process. The specific surface area (S_{BET}) and microporous volume (V_{micro}) were calculated using the BET and t-plot methods, respectively.

2.5 Thermogravimetric Analysis

Thermogravimetric (TG) analyses were carried out on a Mettler-Toledo TG/DSC Star^{e} System apparatus, under air flow, with a heating rate of 5 °C/min from 30 to 800 °C. As mentioned above, before analysis, the samples were hydrated in a 80 % relative humidity atmosphere for 24 h in order to set the hydration state.

3. RESULTS AND DISCUSSION

3.1 Intrusion−Extrusion Isotherms: Pressure−Volume Diagrams

The pressure−volume diagrams of the "Si-FER-$MgCl_2$•$21H_2O$" system are illustrated in Figure 2. Two consecutive intrusion-extrusion cycles were performed and were quite reproducible. As previously reported [8, 9, 12], the volume variations observed below 10 MPa correspond to the compression and filling of the interparticular porosity.

Whatever the intrusion cycle, a marked intrusion step is observed in the range of 150-350 MPa. The intrusion pressure is close to 195 MPa for the first intrusion-extrusion cycle with a total intruded volume of 0.053 mL/g. Such an intruded volume is in quite agreement with the pore volume determined from N_2 physisorption (Vp= 0.13 mL/g, see below) assuming, as shown by Desbiens et al. [39], that the density of the intruded liquid is lower than that of the bulk liquid. The extrusion pressure is shifted to a lower pressure (P_{ext}= 184 MPa) with an extruded volume similar to the intruded one. Thus the "Si-FER-$MgCl_2$•$21H_2O$"system displays a spring behavior with a small hysteresis. It is worthy to note that a pronounced rounding of the transition is observed for the intrusion curve of the second cycle. Such a feature can reveal the presence of few defect sites in the sample after the first intrusion-extrusion cycle, as it was evidenced in Silicalite-1 from a joint experimental and molecular simulation study [7]. These defects, probably silanol groups, would arise from the breaking of siloxane bridges under high pressure. As expected (see Introduction), compared to the "Si-FER-water" system, where the intrusion pressure is close to 150 MPa, the $MgCl_2$ aqueous

solution intrusion occurs at a pressure 30% higher. However it should be noticed that the increase of the intrusion pressure (ΔP = 45 MPa) is relatively low compared to the one observed for the "MFI-type zeosil- $MgCl_2 \bullet 21H_2O$" system (ΔP=85 MPa) [16]. For the"Si-FER- $MgCl_2 \bullet 21H_2O$"system, such an increase cannot be only explained neither by the increase of the surface tension of the $MgCl_2$ solution, which increases by about 12% from pure water [40], nor by the osmotic pressure, which leads to ΔP =25 MPa [25, 26]. It can be supposed, in agreement with the structure refinement (see below), that the intrusion pressure increase (ΔP) is related mainly with the partial desolvation of Mg^{2+} and Cl^- ions.

3.2 XRPD characterizations at ambient conditions

Figure 3 reports the XRPD patterns of Si-FER samples before and after intrusion−extrusion experiments. They are quite similar indicating, at least at the long range order, that the FER structure is preserved after intrusion-extrusion experiments. The absence of strong differences in the peak intensities also suggests that all the solution intruded in the channels was extruded upon pressure release. This is in agreement with the results of the intrusion-extrusion curves, which indicate that the intruded liquid is subsequently expelled from the solid.

3.3 TG analysis and N_2 adsorption-desorption measurements

The TG curves of the Si-FER samples before and after intrusion-extrusion experiments are given in Figure 4. For the non-intruded and intruded-extruded samples one main weight loss close to 2.2 wt.% and 2.6 wt.%, respectively, is observed between room temperature and 800 °C. These weight losses correspond mainly to traces of physisorbed water molecules but also, at higher temperature (>300 °C), to water molecules arising from dehydroxylation reactions (condensation of OH groups). The low difference in weight loss between the two samples (0.4 wt.%), confirms that the creation of defect sites (silanol groups) after intrusion-extrusion

experiment, if any, is very low. Such a result was confirmed by ^{29}Si and ^{1}H-^{29}Si CP MAS NMR experiments (see Figures S1 and S2). The textural properties of the different Si-FER samples were determined from N_2 adsorption-desorption measurements. In order to avoid a dehydroxylation process, the samples were outgassed at 90 °C under vacuum. The isotherms are reported in Figure 5. They are of type I, characteristic of microporous materials. No significant changes are observed between the non-intruded and intruded-extruded samples. In both cases, the micropore volume is quite similar and close to 0.12-0.13 mL/g which is in quite good agreement with the published data [41]. At high relative pressures ($p/p° = 0.95$) and particularly for the intruded-extruded sample, an increase of the adsorbed volume corresponding to an interparticular porosity is observed. Such a porosity might be explained by the breaking of some ferrierite crystals under high pressure.

3.4 In situ high pressure XRPD experiment

Selected patterns collected during the in situ HP synchrotron XRPD experiment are reported in Figure 6. Pressure increase induces the shift of the peak positions, the variations in their intensity ratios (especially at low 2ϑ angles) and the rising of new peaks. While the peak shift is a consequence of the framework deformation as a response to pressure, the variation of their intensity ratio is the first indication of the PTM penetration in the Si-FER porosity, the low 2ϑ region of the pattern being highly sensitive to changes in the extraframework content and distribution [42]. The arise of new peaks (observed from 0.68 GPa) is due to the phase transition from P*mnn* to $P2_1/n$ s.g. This phase transition has been observed in all the high pressure experiments performed on Si-FER, whatever the PTM employed [43].

The unit cell parameters (Table 1, Figure 7) were refined up 1.47 GPa (a higher pressure when compared with that reached in the intrusion-extrusion cycles, i.e. 0.35 GPa) in order to

compare the elastic behavior of Si-FER compressed in the electrolyte solution with that observed for other penetrating aqueous pressure transmitting media. It is well known, in fact, that zeolite compressibility is related to the type and amount of extraframework cations and/or molecules hosted in the channels [44] and, thus, by the penetration of additional cations/PTM molecules during compression.

Figure 7 shows that the volume variations in the P_{amb}-1.5 GPa pressure range of Si-FER compressed in m.e.w [29] and in $MgCl_2$ electrolyte aqueous solution (this work) are comparable: ΔV= -3.20 % and -3.70 %, respectively. A slight increase in *a* parameter is observed at about 0.3 GPa in both experiments, that can be ascribed to the PTM intrusion, as discussed in the following. The most remarkable difference is linked to the increase of the *c* parameter at P>0.68 GPa, observed only in the experiment with $MgCl_2$ aqueous solution.

This could be due to the orthorhombic-monoclinic phase transition. Unfortunately, no detailed structural data are available in this pressure.

The volume variations experienced by Si-FER compressed in these aqueous media are very far from that observed compressing in non-penetrating medium (i.e. silicone oil) [43], (ΔV approximately equal to -10% in the same P range). This largely different elastic behavior is due to the penetration of the medium molecules, which contributes to stiffen the structure. Arletti et al. [29] demonstrated that the low compressibility of Si-FER in m.e.w. is the consequence of the penetration of 15 water molecules in the pores, already at the lowest investigated pressure.

The structural refinement of the "Si-FER- $MgCl_2 \bullet 21H_2O$" system was performed on the data collected at 0.28 GPa, on Si-FER still exhibiting the orthorhombic symmetry. This pattern corresponds to the experimental pressure point nearest to the maximum value reached in the porosimeter intrusion – extrusion cycles (about 0.2 GPa). Observed and calculated patterns are reported in Figure 1.

From the inspection of the residual electron density map, it was possible to locate 0.7 Mg , 2 Cl atoms and 8 water molecules, even if we cannot exclude the presence of other cations and /or water molecules in a disordered configuration. Therefore, the idealized composition of the electrolyte solution inside the porosity is: $MgCl_2 \bullet 10H_2O$. The projections along [001] and [010] of the resulting structure are shown in Figure 8a and b, respectively. Mg atoms are at the center of the FER cage, at the intersection with the 8 MR channel running along [010], coordinating four partially occupied water molecules (W3) in a square planar configuration (Table S3). These W3 molecules are, in turn, bonded to framework oxygen atoms and to another water molecule (W1) sited in the 10 MR channel (Table S3). The position of Mg cation perfectly matches that found by Alberti et al. [45] in natural ferrierite from Monastir (Sardinia – Italy). In the natural sample Mg cations are completely water solvated, coordinated by six water molecules in a perfect octahedral geometry. Otherwise, in our system, considering the partial W3 site occupancy, each Mg cation coordinates only 2.8 water molecules, thus being partially desolvated. Cl^- cations are located in the 10 MR channel running along [001], slightly shifted with respect to the center of the 8 MR channel. Each 10 MR channel hosts one Cl^- cation coordinating one W1 and one W2 water molecule. A symmetrically equivalent W1 molecule (far from Cl) coordinates framework oxygen atoms and one W3 molecule in the FER cage.

Based on recent simulation studies performed by Ge et al. [46], the number of water molecules coordinating Cl^- anions in aqueous solutions is on average equal to 5-6. As observed for Mg cations, these data indicate that, after intrusion into the porosities, also the chlorine anions are partially desolvated, coordinating Cl^- only 2 water molecules. The calculated average value of H-bond distances for $Cl \cdots\cdots H_2O$ molecule is about 3.1 Å [46], that is slightly longer than that found for Cl-W2 bond (2.79(3) Å) in our system. Nevertheless,

in a study of Cl_2 hydrate clathrates, Cl·····H_2O distances range from 2.90 to 3.07 Å [47], in agreement with our results.

The Rietveld analysis supports an idealized composition of the intruded liquid close to $MgCl_2 \bullet 10H_2O$ (5.56 M), that is very close to the concentration of saturated $MgCl_2$ solution. Taken into account the intruded volume determined from the intrusion experiment (V=0.053 mL/g) and the molarity of the intruded liquid (5.56 M), the number of Mg atoms per unit-cell is in good agreement with the value deriving by the Rietveld structural refinement. Unfortunately, it was not possible to refine the structure at higher pressure or upon pressure release to verify whether the framework distortion and the increase of the unit cell *c* parameter, observed after the Si-FER phase transition, could have favored the penetration of further water molecules and/or ions. As a consequence, it is not possible to discuss in details the reversibility of the intrusion – extrusion on the basis of the diffraction data. However, it is worth noting that the pattern collected at P_{amb} after pressure release presents new peaks violating the extinction conditions of $P2_1/n$ *s.g.* and indicating $P2_1$ as the most probable symmetry. This could reveal the occurrence of another phase transition – from $P2_1/n$ to $P2_1$ s.g. – induced at higher pressure and maintained after P release, or generated during decompression. Nevertheless, due to the low quality of the diffraction patterns at very high pressure and to the P-induced crystallization of the PTM, it was possible to argue this second transition only from the inspection of the pattern collected upon pressure release (P_{amb} rev). Being the sample still monoclinic, the framework deformations are still evident in the P_{amb} rev pattern. Due to the low quality of the pattern, it is not possible to do hypothesis regarding the structure once the pressure is released. The results on the reversibility deduced on the basis of the diffraction patterns are not directly comparable to those deriving from the porosimeter experiment, due to the different P_{max} reached in the two experiments (2.6 GPa and 0.35 GPa,

respectively). The higher compression during XRPD experiment could have induced more defects in the Si-FER structure, leading to a partially irreversible behavior.

4. CONCLUSIONS

Intrusion-extrusion experiments of $MgCl_2 \bullet 21H_2O$ (2.65M) aqueous solution were performed in pure silica ferrierite under pressure, and *in situ* HP synchrotron XRPD experiments were carried out to obtain, for the first time to our knowledge, a detailed structural description of the nature and location of the species intruded under pressure in ferrierite porosities using an electrolyte solution as penetrating medium.

The pressure-volume diagram reveals that the intrusion of $MgCl_2$ electrolyte aqueous solution occurs in the range 150-350 MPa. The phenomenon is completely reversible with a small hysteresis observed at the extrusion step, indicating that the "Si-FER- $MgCl_2 \bullet 21H_2O$" system behaves like a spring. Very few defect sites are created after such an experiment. The Rietveld refinement of the XRPD pattern collected at a pressure close to the intrusion one (0.28GPa) shows that the symmetry of Si-FER results to be still orthorhombic P*mnn* and, most important, that both ions and water molecules present in the $MgCl_2$ aqueous solution were intruded in the porosities. However, the solvation degree of the intruded ions differs from the initial solution, revealing a partial desolvation of both magnesium and chloride ions. As a whole, the nature and amount of the intruded species correspond to a $MgCl_2 \bullet 10H_2O$ composition. The lower water content and hence the higher concentration of the intruded solution could be reasonably the result of the hydrophobic nature of the host zeolite matrix.

A phase transition to the monoclinic symmetry $P2_1/n$ is observed for pressure values higher than 0.28 GPa, as already reported for compression experiments of Si-FER with other PTMs

[29, 43]. Upon pressure release from the highest P value to P_{amb}, the system maintains the monoclinic symmetry, but another s.g. ($P2_1$) is argued.

ACKNOWLEDGMENTS

The BM01 beamline at the European Synchrotron Radiation Facility is acknowledged for allocation of experimental beamtime. This work was supported by the Italian MIUR, within the framework of the following projects: PRIN2010-11 ‘‘Dalle materie prime del sistema Terra alle applicazioni tecnologiche: studi cristallochimici e strutturali’’; FIRB, Futuro in Ricerca ‘‘Impose Pressure and Change Technology’’ (RBFR12CLQD).

SUPPLEMENTARY MATERIAL

* Supporting Information

Crystallographic data of Rietveld refinement (refinement parameters (Table S1), coordinates (Table S2), bond distances (Table S3)). ^{29}Si MAS and ^{1}H-^{29}Si CP MAS NMR spectra of the non-intruded and intruded samples (Figures S1 and S2). This material is available free of charge via the Internet at http://pubs.acs.org.

REFERENCES

[1] V. Eroshenko, R.-C. Regis, M. Soulard, J. Patarin, J. Am. Chem. Soc., 123 (2001) 8129 - 8130.

[2] M. Soulard, J. Patarin, V. Eroshenko, R. Regis, In Recent Advances in the Science and Technology of Zeolites and Related Materials: Proceedings of the 1^{4}th International Zeolite Conference; Van Steen, E.; Claeys, M.; Callanan, L. H., Eds.; Studies in Surface

Science and Catalysis, Elsevier: Amsterdam, The Netherlands, 2004; 154, Part B, pp 1830 - 1837.

[3] V. Eroshenko, R. C. Regis, M. Soulard, J. Patarin, C. R. Phys., 3 (2002) 111 - 119.

[4] Y. Lee, J.A. Hriljac, T. Vogt, J. B. Parise, G. Artioli, J. Am. Chem. Soc., 123 (2001) 12732-12733.

[5] Y. Lee, J.A. Hriljac, A. Studer, T. Vogt, Phys. Chem. Miner., 31 (2004) 22-27.

[6] R.W. Washburn, Proc. Nat. Acad. Sci. U.S.A., 7(4) (1921) 115 -116.

[7] M. Trzpit, M. Soulard, J. Patarin, N. Desbiens, F. Cailliez, A. Boutin, I. Demachy, A.H. Fuchs, Langmuir, 23 (2007) 10131–10139.

[8] L. Tzanis, B. Marler, H. Gies, J. Patarin, J. Phys. Chem. C, 117 (2013) 4098–4103.

[9] I. Khay, L. Tzanis, T.J. Daou, H. Nouali, A. Ryzhikov, J. Patarin, Phys. Chem. Chem. Phys., 15 (2013) 20320–20325.

[10] M. Trzpit, S. Rigolet, J.-L. Paillaud, C. Marichal, M. Soulard, J. Patarin, J. Phys. Chem. B, 112 (2008) 7257–7266.

[11] Y. Grosu, G. Renaudin, V. Eroshenko, J.M. Nedelec, J.P.E Grolier, Nanoscale, 7 (2015) 8803–881.

[12] G. Ortiz, H. Nouali, C. Marichal, G. Chaplais, J. Patarin, Phys. Chem. Chem. Phys., 15 (2013) 4888-4891.

[13] I. Khay, G. Chaplais, H. Nouali, C. Marichal, J. Patarin, RSC Advances, 5 (2015) 31514- 31518.

[14] G. Ortiz, H. Nouali, C. Marichal, G. Chaplais J. Patarin, J. Phys. Chem. C, 118 (2014) 21316-21322.

[15] L. Liu, X. Chen, W. Lu, A. Han, Y. Qiao, Phys. Rev. Lett., 102(18) (2009) 184501/1-184501/4.

[16] L. Tzanis, H. Nouali, T.J. Daou, M. Soulard, J. Patarin, Mater. Lett., 115 (2014) 229–232.

[17] I. Khay, T. J. Daou, H. Nouali, A. Ryzhikov, S. Rigolet, J. Patarin, J. Phys. Chem. C, 118 (2014) 3935–3941.

[18] G. Ortiz, H. Nouali, C. Marichal, G. Chaplais J. Patarin, J. Phys. Chem. C, 118 (2014) 7321−7328.

[19] A. Ryzhikov, I. Khay, H. Nouali, T.J. Daou, J. Patarin, Phys. Chem. Chem. Phys., 16 (2014) 17893–17899.

[20] I. Kabalan, I. Khay, H. Nouali, A. Ryzhikov, B. Lebeau, S. Albrecht, S. Rigolet, M.-B. Fadlallah, J. Toufaily, T. Hamiyeh, T., et al., J. Phys. Chem. C., 119 (2015) 18074–18083.

[21] A. Han, Y. Qiao, Appl. Phys. Lett., 91 (2007) 173123–173127.

[22] M. Soulard, J. Patarin, French patent 1154707 (2011).

[23] A. Han, W. Lu, T. Kim, X. Chen, Y. Qiao, Phys. Rev. E: Stat. Phys., Plasmas, Fluids, 78 (2008) 031408–031412.

[24] A. Han, W. Lu, T. Kim, V.K. Punyamurtula, Y. Qiao, Smart Mater. Struct., 19 (2009) 024005–024010.

[25] M. Michelin-Jamois, C. Picard, G. Vigier, E. Charlaix, Phys. Rev. Lett., 115 (2015) 036101−1 – 036101−4.

[26] M. Michelin-Jamois, C. Picard, E. Charlaix, G. Vigier, arXiv:1404.5318v1 [physics.chem-ph] 2014, 1-4.

[27] A. Ryzhikov, L. Ronchi, H. Nouali, T.L. Daou, J.-L. Paillaud, J. Patarin, J. Phys. Chem. C, 119 (2015) 28319−28325.

[28] S. Ori, S. Quartieri, G. Vezzalini, V. Dmitriev, Am. Mineral., 93 (2008) 1393–1403.

[29] R. Arletti, G. Vezzalini, S. Quartieri, F. Di Renzo, V. Dmitriev, Microporous Mesoporous Mater., 191 (2014) 27–37.

[30] C. Baerlocher, L.B. McCusker, B. Olson, W.M. Meier, Atlas of Zeolite Framework Types, Published on behalf of the Structure Commission of the International Zeolite Association by Elsevier, Boston; Amsterdam, 2007.

[31] A. Kuperman, S. Nadimi, S. Oliver, G.A. Ozin, J.M. Garces, M.M. Olken,. Nature, 365 (1993) 239- 241.

[32] R. Miletich, D:R. Allan, W.F. Kuhs, In High- Temperature and High-Pressure Crystal Chemistry, Reviews in Mineralogy and Geochemistry, vol. 41; R.M. Hazen, R.T. Downs, Eds.; Mineralogical Society of America and Geochemical Society: Washington, USA, 2000.

[33] R.A. Forman, G.J. Piermarini, J.D. Barnett, S. Block, Science, 176 (1972) 284-285.

[34] H. K. Mao, J. Xu, P.M. Bell, J. Geophys. Res., 91 (1986) 4673-4676.

[35] A.P. Hammersley, S.O. Svensson, M. Hanfland, A.N. Fitch, D. Hausermann, High Pressure Res., 14 (1996) 235−248.

[36] A.C. Larson, R.B. Von Dreele, General Structure Analysis System “GSAS”; Los Alamos National Laboratory Report; Los Alamos, 1994; LAUR 86-748.

[37] B.H. Toby, J. Appl. Cryst., 34 (2001) 210−213.

[38] P. Thomson, D.E. Cox, J.B. Hastings, J. App. Cryst., 20 (1987) 79–83.

[39] N. Desbiens, I. Demachy, A.H. Fuchs, H. Kirsch-Rodeschini, M. Soulard, J. Patarin, Angew. Chem. Int. Ed., 44 (2005) 5310–5313.

[40] P. Wang, A. Anderko, R.D. Young, Ind. Eng. Chem. Res., 50 (2011) 4086–4098.

[41] G.-Q. Guo, Y.-J. Sun, Y.-C Long, Chem. Commun. (2000) 1893–1894.

[42] R. Arletti, G. Vezzalini, A. Morsli, F. Di Renzo, V. Dmitriev, S. Quartieri, Microporous Mesoporous Mater., 142 (2011) 696-707.

[43] P. Lotti, R. Arletti, G.D. Gatta, S. Quartieri, G. Vezzalini, M. Merlini, V. Dmitriev, M. Hanfland, Microporous Mesoporous Mater., 191 (2014) 27–37.

[44] E. Fois, A. Gamba, G. Tabacchi, R. Arletti, S. Quartieri, G. Vezzalini, Amer. Mineral., 90 (2005) 28-35.

[45] A. Alberti, C. Sabelli, Zeit. Kristallogr., 178 (1987) 249 – 256.

[46] L. Ge, L. Bernasconi, P. Hunt, Phys. Chem. Chem. Phys., 15 (2013) 13169-13183.

[47] K.A., Udachin, S. Alavi, J.A. Ripmeester, J.A., J. Phys. Chem. C, 117 (2013) 14176-14182.

Figure captions

Figure 1. Observed (crossed line) and calculated (continuous line) diffraction patterns – selected angular range - from Rietveld refinements of "Si-FER - $MgCl_2$ aqueous solution" at 0.28 GPa. The short tick marks below the pattern give the position of the Bragg reflections.

Figure 2. Pressure-volume diagrams of the "Si-FER-$MgCl_2$•$21H_2O$"system for 1st and 2nd intrusion-extrusion cycles.

Figure 3. Ex-situ XRPD patterns of the Si-FER samples before (a) and after (b) intrusion−extrusion experiments with $MgCl_2$•$21H_2O$ aqueous solution.

Figure 4. TG curves under air of the Si-FER samples before (a) and after (b) intrusion−extrusion experiments with $MgCl_2$•$21H_2O$ solution.

Figure 5. N_2 adsorption−desorption isotherms at -196 °C of the Si-FER samples outgassed at 90 °C under vacuum: before (a) and after (b) two intrusion-extrusion cycles with $MgCl_2$•$21H_2O$ solution (black squares : adsorption curves; black circles: desorption curves).

Figure 6. Selected in-situ XRPD patterns collected at increasing pressures and upon pressure release (rev).

Figure 7. Variation of lattice parameters a, b, c (Å) and V ($Å^3$) with pressure measured in Si-FER compressed in $MgCl_2$•$21H_2O$ and in methanol:ethanol:water (16:3:1, m.e.w.) [35]. Symbols are the same for all figures. Error bars reports 4σ value.

Figure 8. Structure of Si-FER compressed at 0.28 GPa in $MgCl_2$•$21H_2O$ along [001] (a) and [010] (b). Equivalent unoccupied crystallographic positions are not shown.

Table 1. Unit cell parameters of Si-FER at the investigated pressures using $MgCl_2 \cdot 21H_2O$ as pressure transmitting medium.

Pressure (GPa)	Space Group	a (Å)	b (Å)	c (Å)	V (Å^3)	Beta (°)
P_{amb}	P*mnn*	18.708(1)	14.0690(8)	7.4177(4)	1952.4(2)	
0.15	P*mnn*	18.696(3)	14.071(1)	7.4134(3)	1950.3(6)	
0.28	P*mnn*	18.708(2)	14.042(1)	7.3986(5)	1943.6(4)	
0.68	P$2_1/n$	18.64(6)	13.955(3)	7.369(1)	1917(1)	90.18(3)
0.92	P$2_1/n$	18.543(9)	13.908(4)	7.387(2)	1905(1)	90.22(5)
1.19	P$2_1/n$	18.47(1)	13.869(6)	7.384(3)	1891(2)	90.33(5)
1.47	P$2_1/n$	18.41(1)	13.839(7)	7.378(4)	1880(2)	90.2(1)
P_{amb} *(rev)*	P2_1	18.709(2)	14.038(3)	7.468(1)	1960.2(5)	91.84(2)

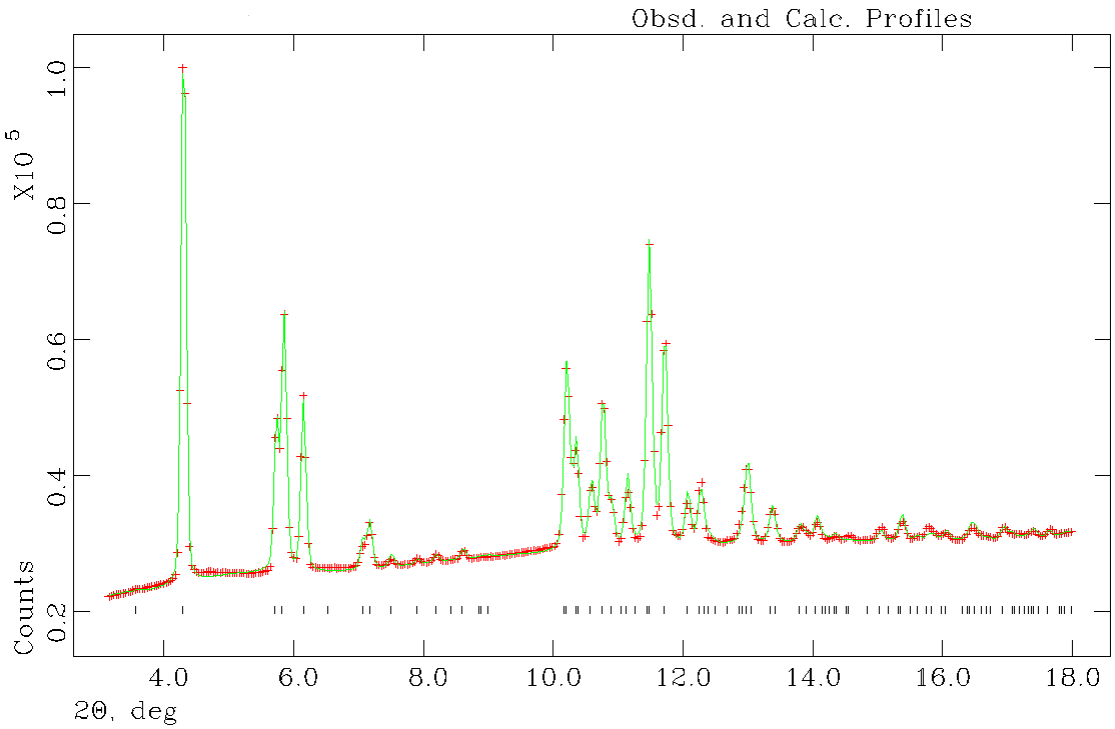

Figure 1. Observed (crossed line) and calculated (continuous line) diffraction patterns – selected angular range - from Rietveld refinements of "Si-FER - $MgCl_2$ aqueous solution" at 0.28 GPa. The short tick marks below the pattern give the position of the Bragg reflections.

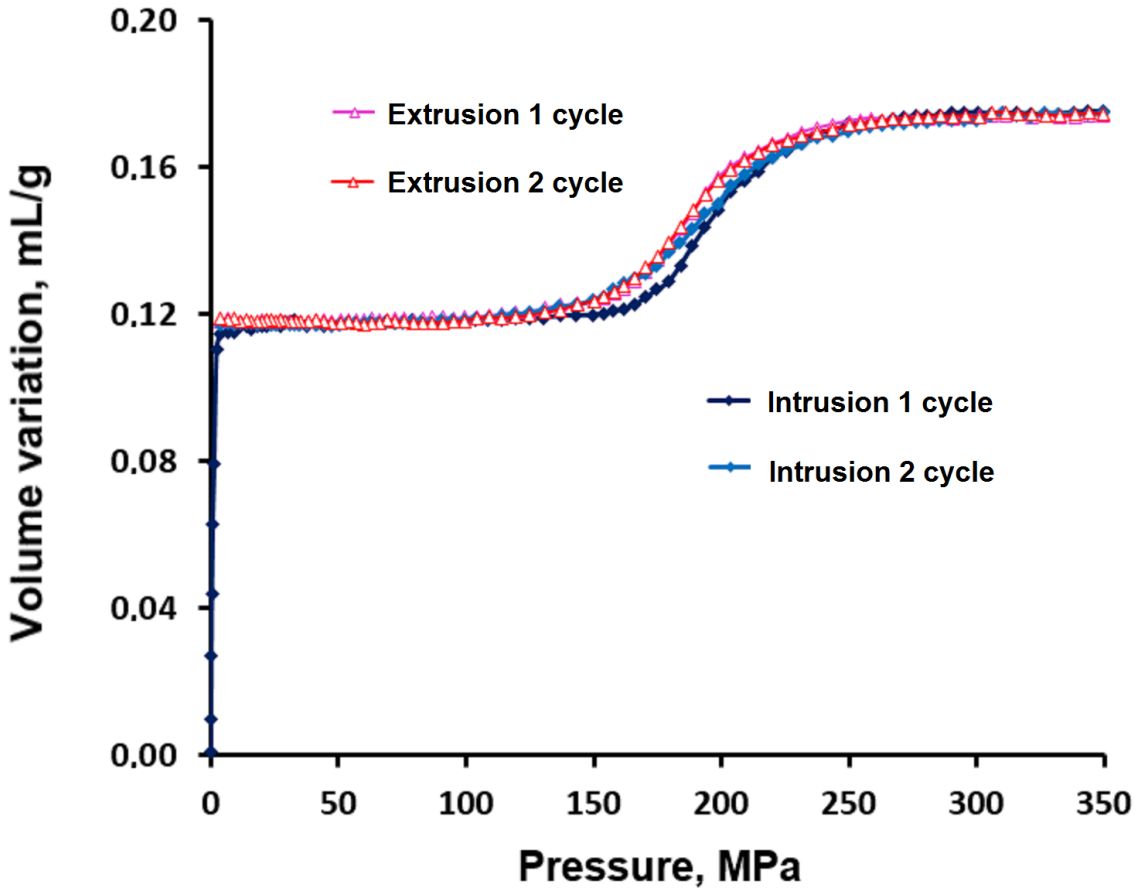

Figure 2. Pressure-volume diagrams of the "Si-FER-$MgCl_2$•$21H_2O$"system for 1st and 2nd intrusion-extrusion cycles.

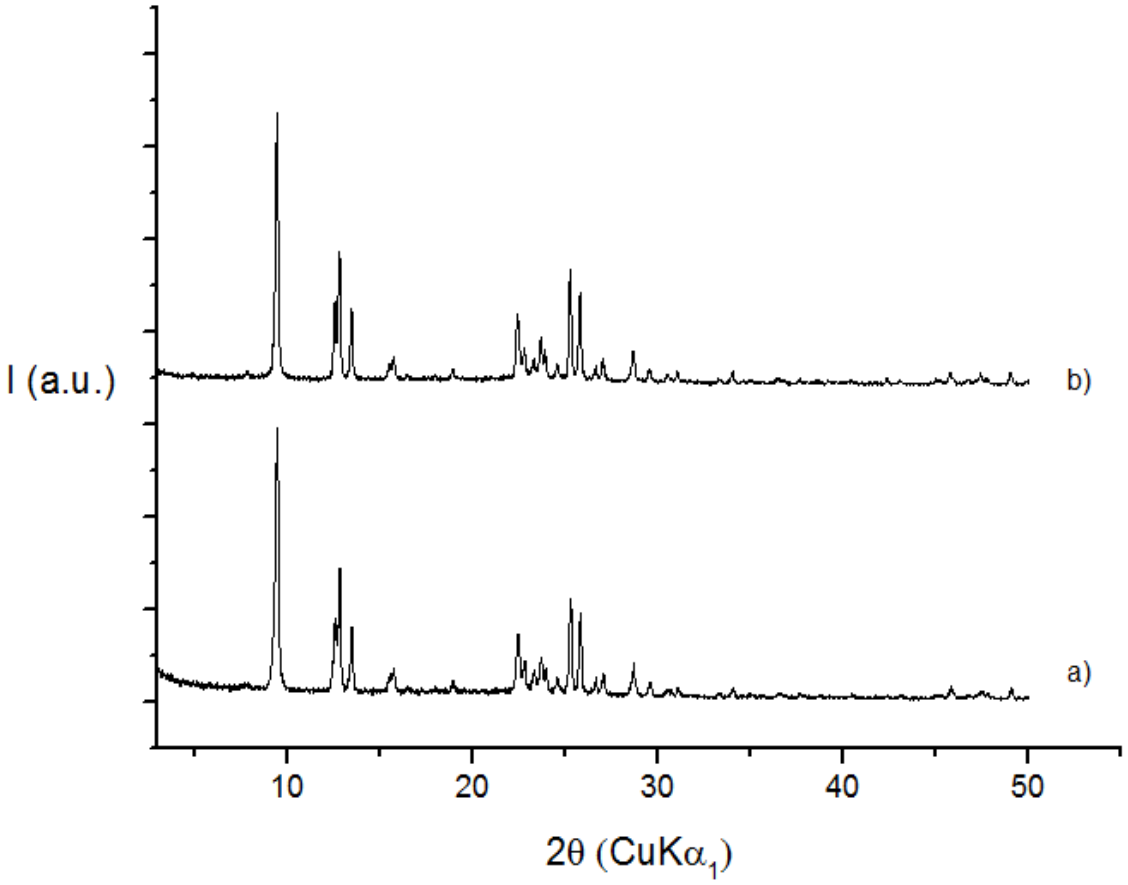

Figure 3. Ex-situ XRPD patterns of the Si-FER samples before (a) and after (b) intrusion−extrusion experiments with $MgCl_2$•$21H_2O$ aqueous solution.

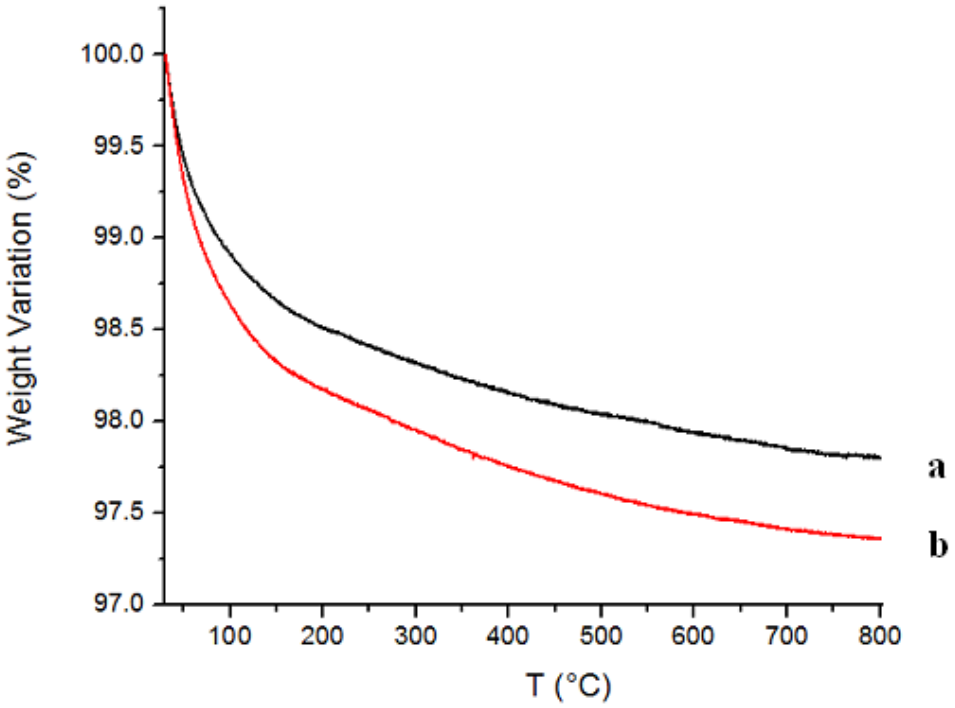

Figure 4. TG curves under air of the Si-FER samples before (a) and after (b) intrusion−extrusion experiments with $MgCl_2$•$21H_2O$ solution.

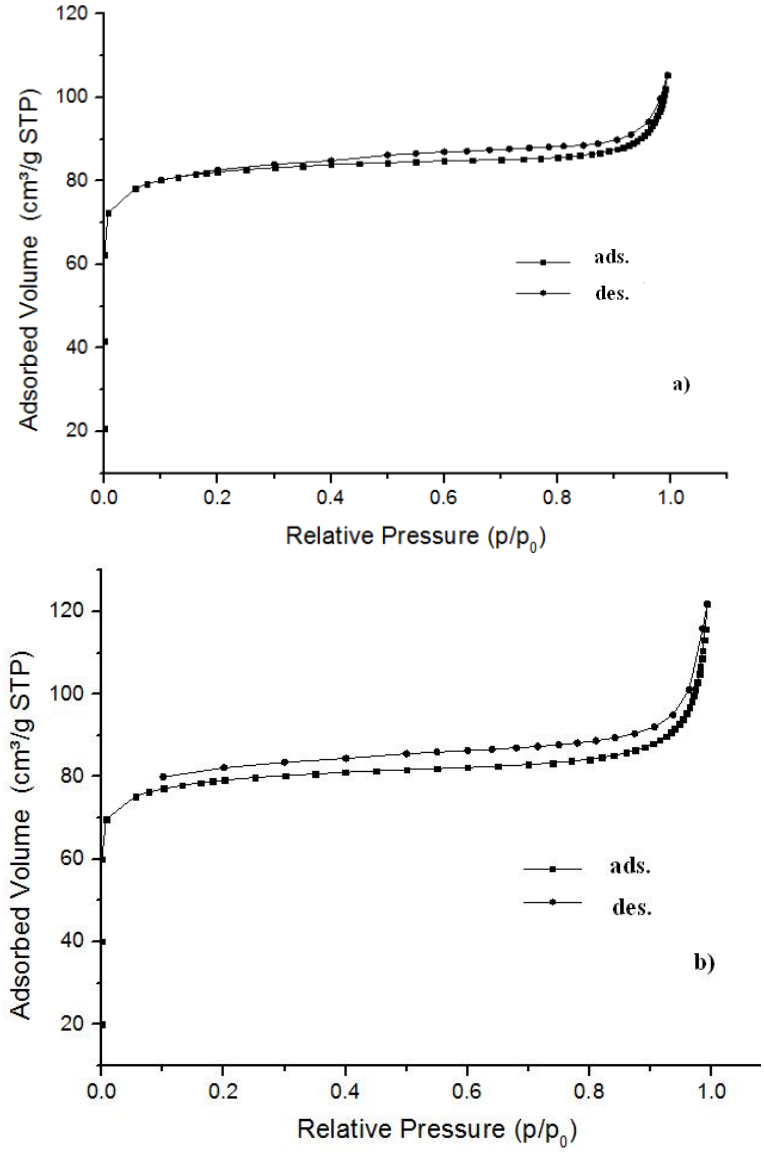

Figure 5. N_2 adsorption−desorption isotherms at -196 °C of the Si-FER samples outgassed at 90 °C under vacuum: before (a) and after (b) two intrusion-extrusion cycles with $MgCl_2$•$21H_2O$ solution (black squares : adsorption curves; black circles: desorption curves).

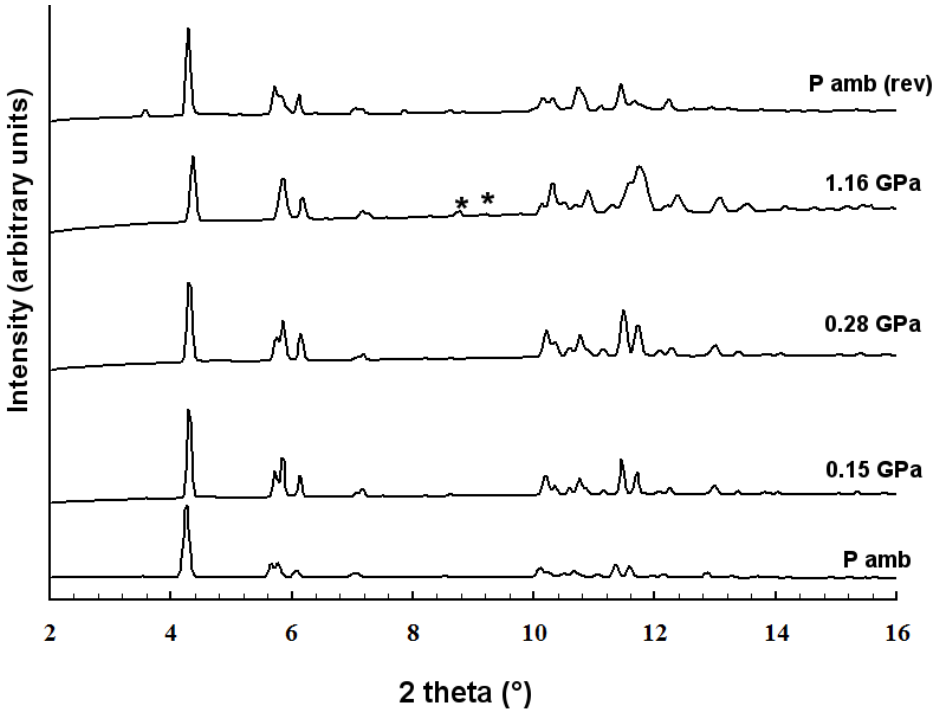

Figure 6. Selected in-situ XRPD patterns collected at increasing pressures and upon pressure release (rev). * indicates the new Bragg peaks arisen after the phase transition to $P2_1/n$.

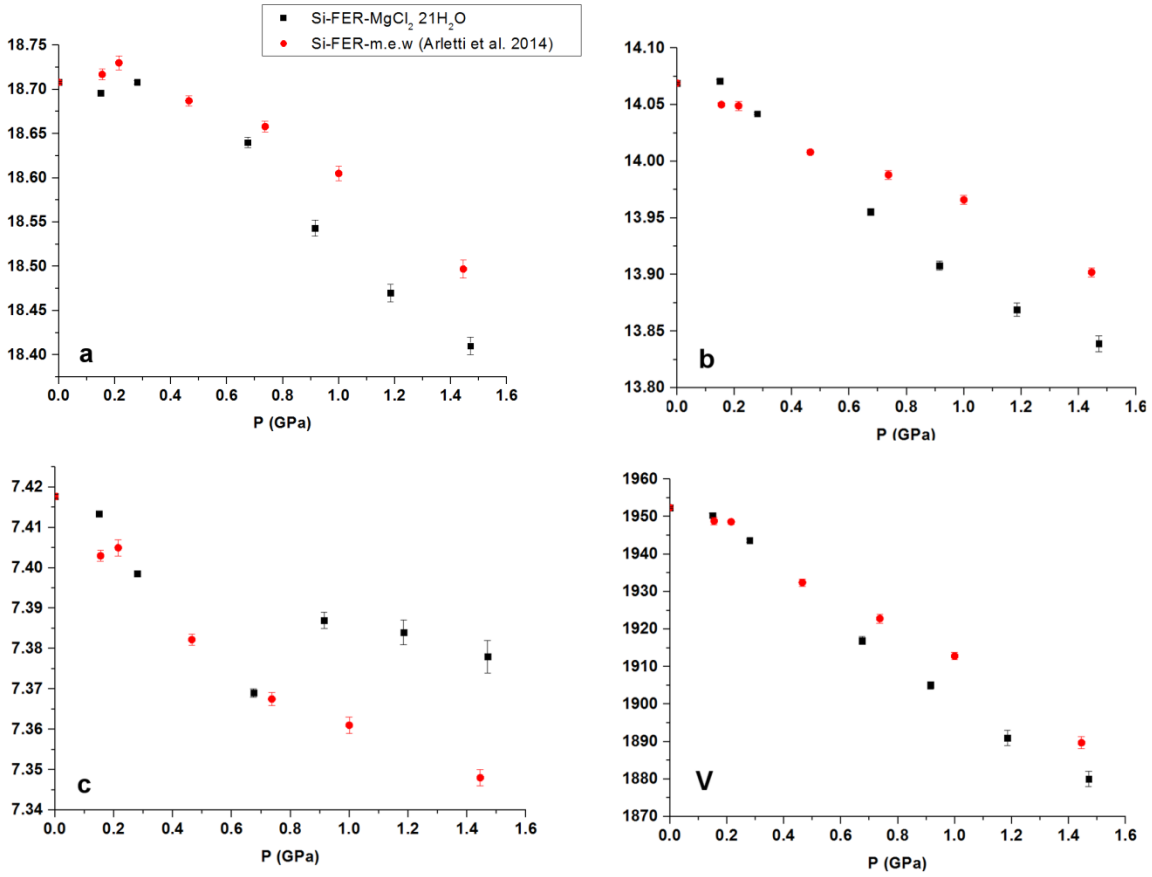

Figure 7. Variation of lattice parameters a, b, c (Å) and V (Å^3) with pressure measured in Si-FER compressed in $MgCl_2$•$21H_2O$ and in methanol:ethanol:water (16:3:1, m.e.w.) [35]. Symbols are the same for all figures. Error bars reports 4σ value.

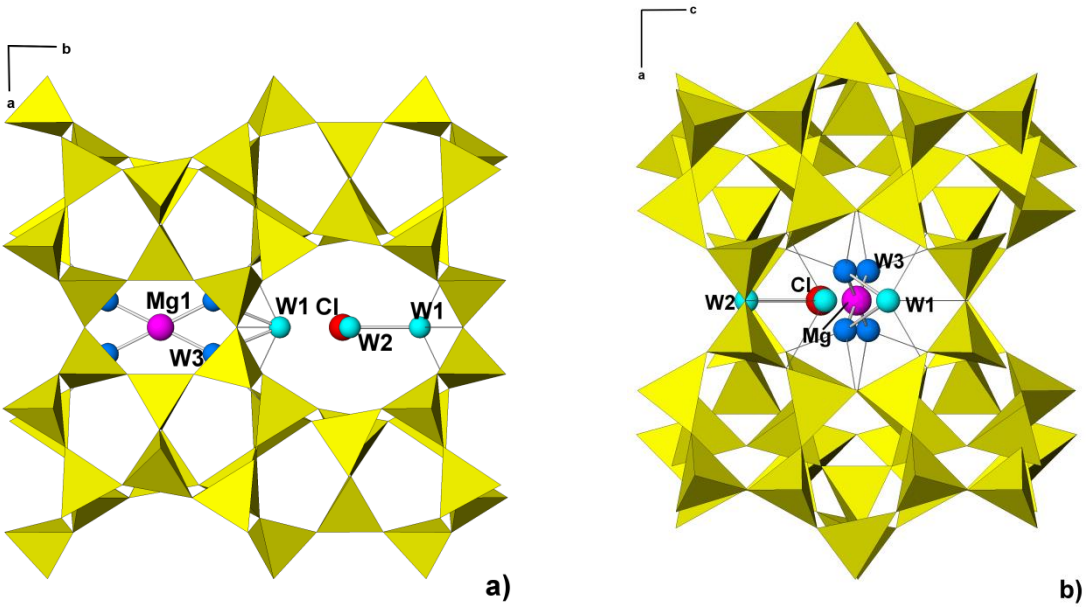

Figure 8. Structure of Si-FER compressed at 0.28 GPa in $MgCl_2$•$21H_2O$ along [001] (a) and [010] (b). Equivalent unoccupied crystallographic positions are not shown.